

Defect formation during growth of hydrogenated amorphous silicon

Gautam Ganguly and Akihisa Matsuda

Electrotechnical Laboratory, Tsukuba City, Ibaraki, 305 Japan

(Received 31 August 1992)

The defects believed to limit the performance of devices fabricated using hydrogenated amorphous silicon are identified as singly occupied dangling bonds. The formation of these defects can be explained on the basis of two distinct models which attribute their occurrence to bulk thermodynamic equilibrium and surface diffusion of precursors during film growth, respectively. We present experimental results on the deposition-rate dependence of electronic and structural properties that are shown to be inconsistent with bulk thermal equilibration. The results, which were anticipated from the surface-diffusion model, are shown to be consistent with the underlying defect-formation mechanism. Simple isotopic substitution of hydrogen is shown to systematically alter the defect-formation rate, providing clear evidence of a surface-controlled defect-formation process during growth of hydrogenated amorphous silicon.

I. INTRODUCTION

The advent of hydrogenated amorphous silicon (*a*-Si:H) as a technologically useful material has relied heavily on the remarkably facile processing technique, radio-frequency (rf, 13.56 MHz) plasma-enhanced chemical-vapor deposition (PECVD).¹ Naturally, a great deal of effort has gone into studies of the plasma and its interaction with the growth surface using *in situ* growth probes.² However, it is only recently that clear evidence has begun to emerge regarding the dominant processes involved.^{3,4} In the meantime, several other deposition techniques—notably, photochemical-vapor deposition (PCVD),⁵ magnetron sputtering (MS),⁶ very high frequency (70~110 MHz) glow discharge deposition,⁷ remote plasma chemical-vapor deposition using a microwave (μ W) source⁸ as well as the hot-wire-assisted CVD method (HWCVD) (Ref. 9) have been developed to a point where the properties of the optimized material resemble that from PECVD. This convergence of properties in material obtained using different processing techniques suggests a common underlying mechanism. The thermodynamic equilibrium (TE) picture of the material structure has been developed to explain why the empirically optimized deposition conditions yield the best material quality.¹⁰ Aesthetically appealing, the picture of thermodynamic equilibrium propagated by hydrogen¹¹ predicts, however, that the material quality cannot be further improved.¹² On the other hand, the surface diffusion (SD) model, which relates the material properties to the diffusion length of precursors on the growth surface,¹³ has led to the improvement of *a*-Si:H-based alloy materials.¹⁴ Introduction of a surface-diffusion mechanism into non-equilibrium growth models has been shown to reduce the bulk defect concentration by a surface smoothening process.¹⁵ Recent time-resolved spectroscopic ellipsometry studies relate the extent of surface smoothening during *a*-Si:H growth with the surface-diffusion length of the precursors and find good agreement with expectations of the SD model on changes of growth conditions.¹⁶ We

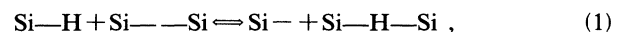
have presented evidence for surface-diffusion length-determined reduction of the bulk defect density in *a*-Si:H deposited at above optimum temperatures.¹⁷ Here, we will set out these results in detail and discuss their implications for the defect formation process.

II. GROWTH PROCESS

In this section we will review the basic concepts of the hydrogen mediated chemical thermodynamics approach on one hand and the surface-diffusion ideas on the other, and see how these can be used to explain the growth condition dependence of the properties of *a*-Si:H. The experimental evidence supporting and contradicting each approach are discussed qualitatively.

A. Thermodynamic equilibrium

The concept of thermodynamic equilibrium was applied to *a*-Si:H to account for the experimentally observed relation between dopant and defect densities.¹⁸ A detailed study of the Fermi energy dependence of defect density, using phosphorus doping during deposition and Li doping after deposition, provided clear evidence for bulk equilibration between dopants and defects.¹⁹ The observation of excess conductivity and electrons in band tail states upon cooling *P*-doped *a*-Si:H from elevated temperatures at faster rates, as compared to slower rates, led to the proposal that hydrogen in *a*-Si:H behaves like a glass.²⁰ Thus, the thermal diffusion of hydrogen becomes sufficient for global equilibration of the silicon network at a temperature which is identified with the glass transition temperature. The microscopic mechanism is envisioned as thermal rupture of Si—H bonds from which hydrogen is emitted into interstitial sites where it is mobile. These hydrogen atoms can insert into strained intersilicon bonds (Si— —Si) as



and by a succession of such steps, effect equilibration be-

tween strained and broken bonds (Si—), i.e., dangling bonds (DB).²¹ As the fraction of Si—H bonds that are broken depends on the temperature, the DB density exhibits a temperature dependence. The activation energy of ~ 0.18 – 0.35 eV (Refs. 21 and 22) is identified with a formation energy. The temperature dependence could be simulated by assuming the above mechanism, with a glass transition or freeze-in temperature of $\sim 200^\circ\text{C}$ for undoped *a*-Si:H.²¹ The thermally driven equilibration mechanisms are expected to be applicable to a set of configurational energy minima which does not include the ground state or crystalline configuration.

These ideas were combined elegantly into the hydrogen chemical potential determined growth model for amorphous silicon.²³ In this model, the hydrogen at Si—H bonding sites are deeply trapped. They can be thermally emitted to states above energy E_M where they are mobile or into shallow trapping states (Si—H—Si) that are identified with the strained intersilicon bonds whose number density decays exponentially from E_M . The hydrogen occupation of these states is determined by the hydrogen chemical potential, μ_H . Consequently, the number of mobile hydrogen atoms

$$N_{HM}(T) = N(E_M) \exp[-\{E_M - \mu_H\}/kT]. \quad (2)$$

μ_H is assumed to equalize across the growth surface between the plasma and the film bulk, providing the connection between changing plasma conditions and the material properties. It is suggested that the as-formed surface structure involves a large density of strained silicon bonds as well as silicon hydrogen bonds. The network relaxes in the subsurface region towards equilibrium, restricted by the temperature-assisted excitation of hydrogen to mobile states. The growth rate determined fraction of hydrogen able to participate in this relaxation process is

$$N_H = \int_{E_R}^{\infty} N_H(E) \exp[-\{E_M - E\}/kT] dE, \quad (3a)$$

where

$$E_M - E_R = kT \ln[\nu_H d_s / \text{growth rate}] \quad (3b)$$

depends on the demarcation energy E_R through the hydrogen hopping frequency (ν_H) and the temperature. The growth zone of thickness d_s is the subsurface region where the hydrogen mediated relaxation takes place. Thus, at optimum growth temperatures of 200 – 300°C , thermal effusion of hydrogen is balanced by in diffusion from the plasma which, it is assumed, leads to μ_H being located at an energy between the Si—H bonding distribution and the shallow trapping states so that an optimum density of both types of trapped hydrogen results. At the same time, the growth rate (~ 1 Å/s) determined E_R [Eq. (3)] is sufficiently deep into the Si—H bonding energy distribution (~ 0.6 eV below E_H , the maximum of the hydrogen bonding distribution)²³ so that a large fraction of the hydrogen can participate in the equilibration process. When the growth rate is increased or the temperature decreased, the number of hydrogen atoms able to participate in the equilibration process decreases and therefore the structure is unable to attain equilibrium [Eq. (3)]. At

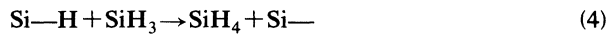
temperatures above the optimum range, the hydrogen thermal evolution rate increases, depopulating the Si—H bonding states and thus forming DB's—as observed experimentally.¹² This scheme predicts that higher growth rates require an increase of the optimum growth temperature which has been demonstrated.¹¹ One experimental result that does not fit into this picture is the effect of heating the *cathode*, in addition to the anode that carries the substrates, in a conventional PECVD system.²⁴ When the opposite electrode is heated, the substrate temperature required to produce optimum quality material is reduced. It appears difficult to attribute this to radiation from the cathode resulting in thermally enhanced hydrogen diffusion because the hydrogen content of the resulting material is independent of the cathode temperature and depends, as in conventional deposition, on the substrate temperature. In the hydrogen-assisted equilibration picture, the way to improve the material quality is to deposit at lower than optimum temperatures and stimulate hydrogen motion nonthermally.²⁵ Lowering the growth rates under these conditions would help allow more hydrogen to diffuse and thus participate in the equilibration process. Improved material is yet to be realized by such a process.

B. Diffusion of precursors on the growth surface

Of the several deposition techniques used for the preparation of *a*-Si:H, the most widespread use is made of the PECVD method and this process is also the best studied in spite of the complexities involved in a reactive plasma. Utilizing the difference between radical and dissociative ionization thresholds, mass spectroscopy suggested that SiH₃ is the dominant neutral species emerging from low-pressure silane discharges.^{26,27} The scavenging effect of NO which reacts with SiH₃ but not with the other possible neutral species was another indirect confirmation of the dominance of SiH₃.²⁸ Subsequently, using high sensitivity, *in situ*, diode laser absorption spectrometry, the concentration of SiH₃ was determined to be $\sim 10^{12}$ cm⁻³,²⁹ which is $\sim 10^{-3}$ of the silane concentration, and orders of magnitude larger than either the ion concentrations ($\sim 10^8$ – 10^9 cm⁻³) measured by mass spectrometry³⁰ or the SiH₂ concentration ($\sim 10^9$ cm⁻³) measured using the ultrasensitive, intracavity laser absorption spectrometry.³¹ The concentration profile of SiH₃ was determined *in a plasma* that produced optimum material quality and was shown to be adequate to explain the film growth rate,³² given a surface sticking probability, $s \sim 0.1$. The surface reaction probability β which is the fraction of incident precursors that remain “physisorbed”³³ on the surface long enough to undergo some reaction, was determined from trench coverage profiles as well as the grid technique to be ~ 0.3 , independent of the substrate temperature in the range from room temperature (RT) to 500°C .³⁴ The deposition rate (without changing plasma conditions) in constant from RT to 300°C , then increases by a factor of ~ 3 up to 450°C and finally saturates. Saturation is associated with all the precursors physisorbed on the surface, contributing to sticking, i.e., growth. Thus, at 480°C , s is set equal to β and its tem-

perature dependence emerges quantitatively from the deposition rate.

Since the hydrogen concentration of the precursors is ~ 30 times that of the bulk material, the hydrogen-rich surface layer loses hydrogen as it becomes a part of the bulk. Hydrogen coverage of the surface during growth over the temperature range RT to 500°C was monitored using *in situ* infrared reflection absorption spectroscopy (IR RAS) (Ref. 35) and also by infrared ellipsometry.³⁶ The temperature dependence of the quantities β and s have been reproduced by a numerical model³⁷ which concludes that the three dominant reactions that the physisorbed precursors undergo while executing thermal hops on the surface from one hydrogenated site to another are the abstraction reaction



which produces a surface DB with a silane molecule being desorbed; the sticking (i.e., growth) reaction



which has a precursor reacting at a hydrogen free or DB site on the surface and the recombination reaction



which releases a disilane molecule to the gas phase. The combination of abstraction and sticking are required for growth—a process requiring two precursors. The precursor recombination reaction (6) affects the concentration of precursors physisorbed on the surface as the sum of the probabilities (P_i) of the three reactions

$$P_a + P_s + P_r = P_t, \quad (7)$$

where the subscripts a , s , and r of P represent reactions 4, 5, and 6, respectively, are equivalent to β and therefore independent of temperature. The reactions become temperature dependent through the diffusion coefficient of the precursors

$$D_s = D_{s0} \exp\{-E_s/kT\} \quad (8)$$

on the surface, where $E_s \sim 0.2\text{--}0.3$ eV.³⁷ Thus, at optimum temperatures, the diffusion coefficient determined diffusion length

$$l = [2D_s\tau_s]^{1/2}, \quad (9)$$

where τ_s is the staying time of the precursor on the surface and is sufficient to locate optimum growth sites. As the temperature is lowered, the movement of the precursors becomes sluggish i.e., D_s decreases. Therefore, l decreases and poor quality material is formed. Above optimum growth temperatures, the surface hydrogen begins to desorb, thus creating surface DB's which reduce τ_s and, hence, l . Thus, the reduction of l at temperatures below and above the optimum range is due to a decrease of D_s and τ_s , respectively. Recent spectroscopic ellipsometry studies of the surface smoothing effect after growth of an interface layer on the substrate was correlated with l , which was shown to vary with substrate temperature in the above described fashion.¹⁶

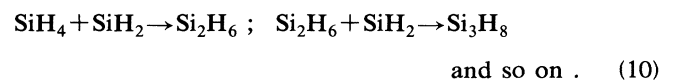
A high activation energy (~ 1.3 eV) for desorption of surface hydrogen can be inferred from the rapid increase of the sticking coefficient s above 350°C compared to the weaker temperature dependence (~ 0.02 eV) of the bulk hydrogen content.³⁸ Since the evolution of bulk hydrogen involves the formation of a silicon-silicon bond in addition to a H—H bond on breaking two Si—H bonds, while on the surface this cannot occur, the difference in activation energies is expected.²¹ This has since been confirmed using *in situ* IR RAS of the surface and bulk hydrogen during and after stopping growth.³⁵ The cathode heating experimental results²⁴ can be explained as being due to an increase of the gas-phase (rotational) temperature of the precursors. This leads to their having greater surface-diffusion length and hence to a better structure and properties in films deposited at low substrate temperatures. The hydrogen content is not affected by the cathode temperature because it depends on the film bulk temperature which is determined by the substrate temperature. The model based upon surface diffusion of the growth precursor can be extended to include the effects of impinging ions (dependent on their number density and energy distribution) or a mixture of different precursors (having different surface reaction and sticking probabilities) on the growth process. Techniques such as MS have been shown to involve large surface reaction probabilities and yet are able to prepare reasonably good material with the help of suitable ion bombardment.³⁹ The deposition techniques that come within the realm of the present model are PCVD and PECVD.

III. EXPERIMENT

In this section, a description of the deposition conditions along with the reasons for their selection is given. The defect density characterization techniques and its calibration are discussed in detail.

A. Deposition conditions

A standard, all stainless steel, PECVD system that can be pumped down to $1\sim 3 \times 10^{-7}$ Torr was used to prepare the films. A relatively low pressure of 30 mTorr was used for depositions from pure silane (SiH_4) or deuterated silane (SiD_4), while for hydrogen diluted mixtures ($\text{H}_2/\text{SiH}_4 \sim 1\text{--}5$), a higher total pressure of 100 mTorr was used. These low silane partial pressures are common to those plasmas used to characterize the radical concentrations³² and yield high-quality α -SiH films under low power conditions. The use of higher pressures lead to formation of powder in the plasma which we believe begins with the formation of higher silanes through successive insertion reactions of the type



When using low-pressure conditions, the ion energies are relatively higher due to the increase in the mean free path. However, the ratio of the number density of ions to neutral radicals remains unchanged (at $< 1\%$ as mentioned in Sec. II B) and their contribution is consequently

considered negligible. The power applied to the cathode ($\sim 76 \text{ cm}^2$) was varied from 2–200 W with the cathode-anode distance fixed at 40 mm, and the flow rate was increased with power from 0.3 to 10 SCCM (cubic centimeter per minute at STP). The electron density increases with power but not its energy distribution and, therefore, the ratio of neutral radicals to ions remains unchanged. The reason for the progressive increase of the flow rate with power is to avoid silane depletion on one hand and formation of higher silanes on the other.⁴⁰ At high applied power with insufficient flow rates, silane is depleted. The radical SiH_2 is generated from and reacts with silane. When the silane partial pressure is reduced by dissociation that generates SiH_2 , its contribution to growth (relative to SiH_3) may increase. The high reactivity (it can insert into a Si—H bond to form Si— SiH_3) and consequent lack of surface mobility of this precursor leads to poorer material quality. If the flow rate is too high relative to the applied power, higher silanes are formed in larger proportions by reaction 10, and precursors formed from their dissociation contribute to growth. The effects of these precursors are detrimental to the material properties. However, the optimum flow rate was not determined for each power condition, and contributions of SiH_2 and higher silane-related precursors vary, thus leading to scatter in the data. The deposition temperature has been monitored using two thermocouples—one placed on the substrate mask (substrate temperature) and the other inside the anode, near the heater (anode temperature). The difference between these two did not always remain constant, especially at higher substrate temperatures due to the low pressures used, and is another source of scatter in the data.

B. Characterization procedure

The dark conductivity, excess conductivity under AM1 (100 mW/cm^2) illumination as well as under an illumination of $\sim 10^{14}$ photons/ cm^2 at 700 nm, optical band gap, refractive index, and hydrogen content (from infrared spectra) have been obtained for all the films studied. Secondary-ion mass spectroscopy has been used to estimate impurity concentrations, Raman scattering for the silicon network structure, and nuclear magnetic resonance (NMR) for the hydrogen bonding distribution. The details of these measurements will be reported separately and we will only discuss comparisons between samples prepared at different substrate temperatures.

The bulk defect absorption has been obtained from the absorption spectra obtained by photocurrent measurements in the constant photocurrent mode (CPM), calibrated by direct transmission measurements near the band gap. To convert the average excess absorption into defect densities, CPM and electron spin resonance (ESR) measurements were carried out on a series of samples of different thickness (1–14 μm). The ESR measurements were carried out at room temperature with 9 ($10 \times 5 \text{ mm}^2$) pieces of the sample, deposited on quartz substrates, fitted snugly into the quartz tube that was always placed at the same position within the cavity. The effects of signal saturation and modulation broadening were as-

certained to select conditions for comparative measurements. Repeated measurements after removing and reinstalling the pieces yielded reproducibility within 1%. The CPM measurements were made on samples with coplanar aluminum electrodes on the top surface, using fields of 10^3 – 10^4 V/cm after checking for Ohmicity. The electrode gap was 0.2 mm, which is small enough to minimize the multiple reflection problems observed with larger spacing.⁴¹ The effect of changing the value of the constant photocurrent and the applied field were ascertained to be small.

There have been several calibration constants (CC) relating the sub-band-gap absorption coefficient to spin densities.^{42–45} They differ in ways of obtaining the defect absorption from the CPM spectrum and the sample conditions for measurement of the spin density. One procedure common to most groups assumes that light-soaked samples consist of mainly bulk spins.⁴² However, it has been shown that the surface spins increase more rapidly than bulk spins with light soaking,⁴⁶ which leads them to overestimate the CC value for calculating bulk spins. One group⁴⁵ calculated the bulk defect densities from CPM independently, using a thickness series and an assumed density of states at the band edge following Ref. 43. This value agrees with the ESR measured bulk spin density to within 11%. Thus, subtraction of the surface spin density allows a more direct comparison between the techniques. An ambiguity in the ESR measurements using a thickness series arises from a shift of the Fermi level that is sometimes observed in thick samples⁴⁷ and casts doubts on spin-density measurements that use only one (thick) sample.²² Measurement of the dark conductivity and the intensity dependence of the photocurrent have been used to confirm that the Fermi energy and hence the defect occupancy does not depend on sample thickness. There is a remaining ambiguity in the ESR calibration itself resulting from a change in cavity Q between standard and sample as well as due to a radial variation of the magnetic-field intensity within the cavity. This implies that the CPM-ESR calibration that identifies the defect absorption with DB's is valid to within a factor of 2. This calibration does not rule out defects other than neutral DB's contributing to CPM measured defect absorption but merely assumes that the ratio remains unchanged. This appears to be reasonable given the agreement between our results and those of Ref. 45, in spite of the different deposition temperatures and other conditions used.

IV. RESULTS

In this section the effects of varying the deposition rate on the material deposited at different temperatures is detailed. Several measurements have been made that compare the properties of the best material deposited at different substrate temperatures.

A. Hydrogenated amorphous silicon

The defect density obtained from calibrated CPM spectra are plotted in Fig. 1 for samples prepared at 250, 400,

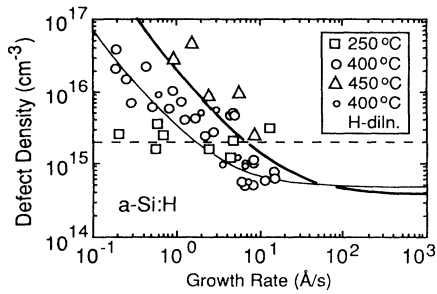


FIG. 1. The defect density in films prepared from pure silane and hydrogen-diluted silane at different growth rates at the indicated substrate temperatures. The lines are calculated defect densities at 400°C (—), 450°C (—), and the assumed average defect density at 250°C (---).

and 450°C as a function of the deposition rate. While the defect density is practically independent of the deposition rate at 250°C, it decreases with increasing deposition rate at the higher substrate temperatures. The calibration of defect densities has been done using the comparison of ESR and CPM data on a series of samples as shown in Fig. 2(a) for samples deposited at 400°C with a deposition rate of ~ 5 Å/s. It is seen in Fig. 2(b) that the defect absorption does not depend on sample thickness from 1–10 μm . The slope of the areal defect density ($\sim 4.2 \times 10^{15} \text{ cm}^{-3}$) and of the defect absorption (0.468 cm^{-1}) versus sample thickness that is shown in Fig. 2(a) gives a calibration constant for the average excess absorption of N_d

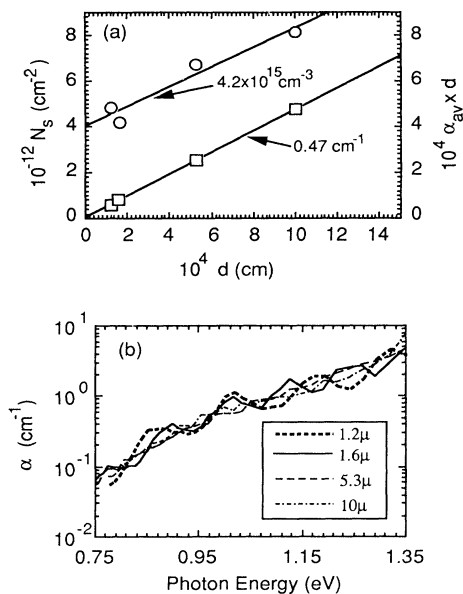


FIG. 2. (a) The areal spin density measured by ESR (\circ) and defect absorption from CPM spectra (\square) for a series of films of different thickness prepared at a growth rate of ~ 5 Å/s at 400°C. The lines are best fits to the data and the indicated values are the slopes corresponding to the bulk values. (b) The CPM measured absorption spectra in the defect absorption region for the same films as in (a) having the indicated thicknesses.

(cm^{-3}) $\approx 1 \times 10^{16} \text{ cm}^{-2} (\alpha_{av}) \text{ cm}^{-1}$ to within 10%. The intercepts for ESR and CPM measured defect densities in Fig. 2(a) illustrate the difference between the techniques—the former being sensitive to all and the latter to only bulk defects. We can compare this calibration to the one obtained in Ref. 42. Using their method of integration gives us a calibration factor of $\approx 8 \times 10^{15} \text{ cm}^{-2} \text{ eV}^{-1}$ while they obtained a value of $\approx 1.9 \times 10^{16} \text{ cm}^{-2} \text{ eV}^{-1}$. The factor of ≈ 2.5 difference is likely to be due to the surface spin contribution that they neglected.

It can be seen in Fig. 1 that some of the fastest grown samples deposited at 400°C have defect densities of $\sim 10^{14} \text{ cm}^{-3}$ which is less than what is obtained at 250°C. We have measured the ESR spin densities of a thickness series prepared using a deposition rate ~ 9 Å/s. This result is plotted in Fig. 3(a) and demonstrates that the bulk spin density is reduced below 10^{15} cm^{-3} . However, the thickness range is an order of magnitude too small to obtain accurate estimates of the bulk spin-density value. To confirm that these ESR results are not influenced by shift of the Fermi level, dark conductivity (σ) and intensity dependence of photoconductivity ($\gamma: \sigma_p \sim F^\gamma$ where F is the light intensity and σ_p is the photoconductivity) data for the samples used in Figs. 2(a) and 3(a) have been shown in Figs. 3(b) and 3(c). Figures 2 and 3 in combina-

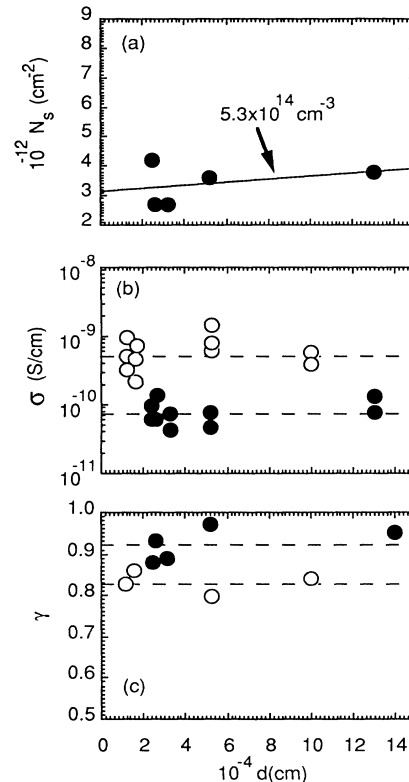


FIG. 3. (a) The areal spin density measured by ESR in films of different thickness prepared at a growth rate of ~ 9 Å/s at 400°C. The line indicates a least-squares fit to the data and the value is the bulk spin density. (b) Dark conductivities of the films shown in Figs. 2(a) (\circ) and 3(a) (\bullet). (c) Index of the intensity dependence of the photoconductivity for the same films as in (b). Dashed lines are guides to the eye.

tion validate the defect estimation procedure for the data in Fig. 1. As mentioned earlier, previously reported²² measurements of defect densities $\sim 10^{14} \text{ cm}^{-3}$ did not ascertain the effects of Fermi-level shifts must therefore be considered unreliable.

The defect densities of the samples used in Fig. 1 have been plotted as a function of the slope of the exponential absorption tail E_u in Fig. 4. The values of E_u decrease with the defect density. In contrast, the transverse-optical-like full width at half maximum of the Raman mode ($\sim 65 \text{ cm}^{-1}$) does not show any variation with deposition rate at 400°C or when the substrate temperature is lowered at 250°C . The optical (Tauc's) gaps of these films show no systematic correlation with hydrogen content,¹⁷ similar to the high-temperature material deposited by the hot wire technique.⁹ The refractive index of the material increases slightly from ~ 3.45 to ~ 3.6 with an increase of deposition temperature and shows a weak decrease of ~ 0.1 with an increase of deposition rate. The hydrogen contents of the films deposited at 250 , 400 , and 450°C are ~ 10 , 3 , and $2 (\pm 1)$ at % respectively, showing no systematic variation with the deposition rate as we have reported previously.¹⁷ The mean peak position of the stretching mode shifts from $\sim 2010 \text{ cm}^{-1}$ in 250°C deposited material to $\sim 2000 \text{ cm}^{-1}$ in 400 or 450°C deposited material. However, the NMR spectra of the films made at 400°C exhibit both narrow and broad components as in material made at 250°C . The difference is a decrease of hydrogen content in both components but more strongly in the broad component. Thus the hydrogen content in the broad line to the narrow decreases from 3:2 in 250°C deposited material to 1:1 in 400°C deposited material. The time-of-flight (TOF) mobilities for electrons and holes have been measured in Au/*a*-Si:H/*c*-Si/Au Schottky structures to be similar in the low defect density material deposited at 250 , 400 , and 450°C . However, with increase of deposition rate, the room-temperature dark conductivity of all films tend to decrease from 10^{-9} to 10^{-12} S/cm with the corresponding AM1 (100 mW/cm^{-2}) photoconductivities going from 10^{-4} to 10^{-6} S/cm , keeping a constant gain. The trend of decreasing dark conductivity with increasing deposition rate appears to correlate weakly with the oxygen content ($\sim 10^{19} \text{ cm}^{-3}$) in the films which tends to decrease by a factor of ~ 2 with increase of deposition rate by an order of magnitude.

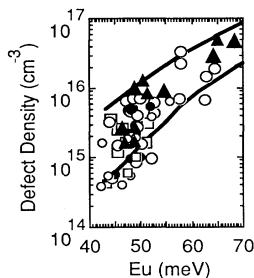


FIG. 4. The defect densities for all films in this study plotted vs the exponential absorption edge slope. The lines are replotted from Fig. 12 of Ref. 21 and correspond to equilibration temperatures of 400 K (upper) and 200 K (lower).

B. Deuterated amorphous silicon (*a*-Si:D)

The growth rates of *a*-Si:D films prepared at different substrate temperatures under constant plasma conditions from SiH_4 and SiD_4 show similar trends but the temperature at which the deposition rate begins to increase is shifted up to 50°C for the deuterated material.¹⁷ This implies (from the discussion in Sec. II B) that the thermal depletion of surface deuterium occurs slowly compared to hydrogen. A similar effect was observed during silicon epitaxy on changing from a hydrogenated to a deuterated surface.⁴⁸ The effect of this isotopic shift on the defect density is shown for deuterated films deposited at 400°C and 450°C at different deposition rates in Fig. 5. In comparing with Fig. 1 we see that the defect densities are significantly lower in the deuterated material compared to the hydrogenated material for the same deposition rates. In fact, the 450°C deposited deuterated films are similar to the 400°C deposited hydrogenated material. The other properties of the deuterated material being quite similar to the hydrogenated one, we will not present these in detail here.

V. DISCUSSION

The results of Fig. 1 show clearly that the defect density in *a*-Si:H does not always increase with increasing power density, or its consequence, the deposition rate. Such a trend is obtainable only under conditions that seek to maintain SiH_3 as the predominant precursors to film growth. We have sought to do this by adjusting the flow rate to match the power density. The reasons for this have been discussed in Sec. II B and it follows that previous studies which reported increase of defect density with deposition rate⁴⁹ worked at high total pressures and, conversely, those that did manage to keep the defect density down even at high deposition rates used low silane partial pressure conditions⁵⁰ to predominantly generate SiH_3 . The deposition rate independent defect density obtained for 250°C deposited material can be understood in terms of the DB creation [Eq. (4)] and saturation [Eq. (5)] reactions on the growth surface. In the steady state, there is no change of the DB concentration on the surface and this concentration is determined by the relative rates of creation and saturation. Thus,

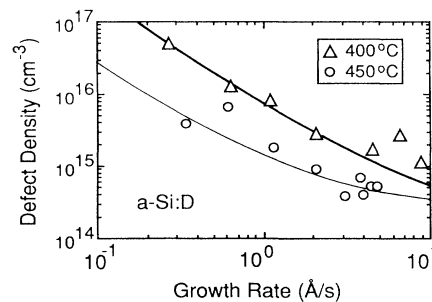


FIG. 5. The defect density in films prepared from deuterated silane at different growth rates at the indicated temperatures. The lines are calculated defect densities at 400°C (—) and 450°C (—) (see text).

$$dN_s/dt = C_a(T)N_H\theta_s - C_s(T)N_s\theta_s = 0, \quad (11)$$

where C_a ($\sim 1/l$) and C_s ($\sim l$) represent the rate constants for abstraction and sticking, respectively, both of which become temperature dependent through the surface diffusion length l [Eq. (9)]. θ_s represents the concentration of SiH_3 on the surface that is determined by the flux and the total surface reaction probability P_t defined by Eq. (7). N_H and N_s represent the number density of hydrogenated and bare (DB) surface sites per unit area whose sum is N_0 . Thus,

$$N_s = [C_a(T)/C_a(T) + C_s(T)]N_0. \quad (12)$$

It is easy to see from Eq. (12) that if only these processes determine the DB density on the surface then this density is independent of the flux or surface concentration of precursors. At this point we introduce the proposal that *the DB density in the bulk of PECVD $a\text{-Si:H}$ films are determined by the steady-state DB density on the surface during growth*. This is a reasonable assumption considering that the surface layer at an instant during film growth becomes a part of the bulk at a later instant. Thus, the defects on each surface layer statistically become a part of the bulk of $a\text{-Si:H}$. This explains why the defect density in the bulk of $a\text{-Si:H}$ is independent of deposition rate at 250°C as shown in Fig. 1 for films prepared under conditions where SiH_3 are the major growth precursors.

In Eq. (12) the surface DB density is a fraction of the total surface site density. This fraction is determined by the abstraction and sticking rate constants of the precursors on the surface. N_s is inversely proportional to the rate constant for sticking which is determined by the diffusion length l of the precursors on the surface [see Eqs. (8) and (9)]. D_s (and, consequently, l) increases with temperature and, therefore, N_s decreases with increasing temperature from RT to 250°C. At the same time, N_s is proportional to the abstraction rate which is determined by the reciprocal of the diffusion coefficient that determines the time spent by the radical at each site. The higher the diffusion coefficient, the shorter the staying time on a single site and hence the lower the abstraction probability. It must be noted, however, that the abstraction process itself must be activated, albeit with an activation energy smaller than the diffusion coefficient which gives $C_a(T)$ a net negative activation energy. Consequently, at low temperatures, C_s becomes smaller while C_a increases and according to Eq. (12) a larger fraction of the surface sites become DB's. Thus, we have a clear correlation between the surface diffusion length l [Eq. (9)] and the DB density, depending on the temperature. This is illustrated in Figs. 6(a) and 6(b) for low (RT) and intermediate (250°C) temperatures, respectively.

At temperatures above 350°C, the increase of DB sites on the surface by thermal desorption of hydrogen⁴ alters the surface DB density and this can be written as

$$dN_s/dt = C_H(T)(N_H)^2, \quad (13)$$

where we assume a bimolecular process. The rate constant C_H which has a strong temperature dependence (~ 1.3 eV) increases by three orders of magnitude be-

tween 250°C and 400°C. As a consequence, the important processes for creation and saturation of surface DB's are quite different at 400°C. In the steady state we have

$$dN_s/dt = C_H(T)(N_H)^2 + C_a(T)N_H\theta_s - C_s(T)N_s\theta_s = 0. \quad (14)$$

This equation shows that the DB concentration on the surface depends on the relative importance of the first and second DB creation terms on the right-hand side. At low θ_s , i.e., low deposition rates, we have

$$N_s \approx C_H(T)N_0^2 / C_s(T)\theta_s, \quad (15)$$

which neglects the precursor abstraction term in comparison to thermal creation as well as N_s in comparison to N_0 , and implies that N_s is inversely proportional to the concentration of precursors on the surface at a constant temperature above 350°C. The physical idea is illustrated in Fig. 6(c) which represents precursors saturating the DB's being created thermally on the surface. If the precursor flux is increased, fewer DB's can be formed in the time required to grow a monolayer. This is consistent with a decreasing defect density with increase in the

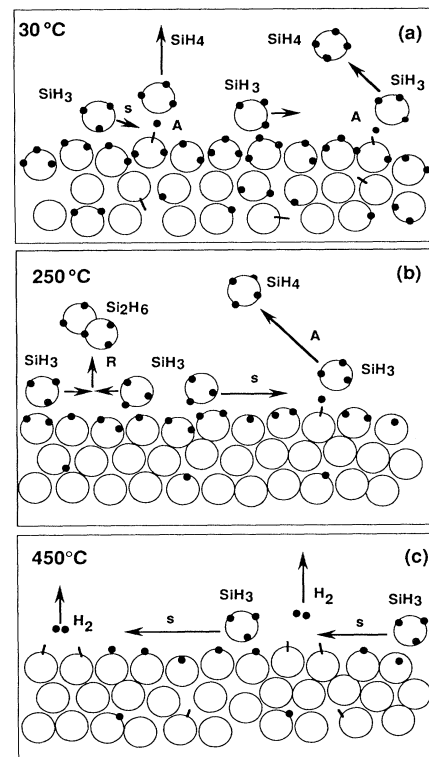


FIG. 6. Schematic representation of the growth surface region of $a\text{-Si:H}$ at (a) room temperature, (b) 250°C and (c) 450°C. The characters A , S , and R stand for the processes defined by Eqs. (4), (5), and (6) in the text. Note that the surface hydrogen bonding configurations, bulk hydrogen contents, and dangling-bond densities are realistic only comparatively between (a), (b), and (c). The arrows indicating movement of SiH_3 on the surface have lengths indicating relative diffusion lengths on the surface (see text).

deposition rate as seen in 400 °C and 450 °C deposited *a*-Si:H samples (Fig. 1). It is interesting to note that the hot wire CVD method using lower ("enough to minimize gas-phase collisions before precursors hit the substrate") pressures and higher deposition rates (5–10 Å/s) results in better quality material at higher temperatures (> 250 °C) compared to PECVD (1.5–2.5 Å/s).¹² It is not known what the growth precursors are in the HWCVD method at such low pressures but the concurrence of results is suggestive.

We see in Eq. (14) that as θ_s increases at 400 °C, the sticking and abstraction rates increase until a point is reached where the abstraction reaction rate is comparable to the thermal desorption rate and eventually exceeds it. Under these conditions the value of N_s is again determined by Eq. (12). The value of C_s is thermally enhanced at 400 °C compared to 250 °C while the value of C_a is reduced. Assuming that the reduction is related through an activation energy $E_s \sim 0.3$ eV for the precursor diffusion coefficient³⁷ and that a flux density of 5×10^{15} cm⁻² corresponds to a deposition rate of 1 Å/s with $s \sim 0.1$ ³² (independent of flux and temperature), we have fitted using Eq. (14) the variation of the defect density as a function of the deposition rate at 400 and 450 °C. This is shown by the lighter and heavier curves, respectively, in Fig. 1 along with an assumed average defect density of 2×10^{15} cm⁻³ at 250 °C. Thus, at 250 °C, the surface DB density is $\sim 10^{-5}$ of the surface site density, which is assumed to be 10^{10} cm⁻². At 400 °C, the surface DB density decreases from 10^{11} cm⁻² at a deposition rate of 0.1 Å/s to 10^9 cm⁻² at 10 Å/s. A transition from the regime of Eq. (14) to Eq. (12) leads to a minimum defect density at deposition rates of ~ 10 Å/s. At 400 and 450 °C the sticking coefficient, s depends on deposition rate due to changes in surface hydrogen coverage. This variation can be up to a factor of 3 since s increases from 0.1 to 0.3 from 300 to 500 °C.³⁴ Considering that this change has been neglected, the fit to the data for two temperatures is rather good. The calculated line in Fig. 1 shows that the minimum DB density value is lower at 450 °C than at 400 °C (due to the activated diffusion coefficient), but occurs at significantly higher deposition rates (due to the much more strongly activated surface bonded hydrogen desorption process) which are not easily attained.

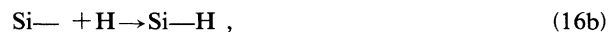
As there are technical problems to further increase of the power density,⁵¹ an alternative method of enhancing precursor diffusion length was attempted. This is based on the effect of isotope substitution on the thermal effusion rate of hydrogen. The lower deposition rate but similar activation energy (~ 1.3 eV) implies that the rate constant for thermal effusion given in Eq. (15) is smaller for deuterium because of a lower attempt frequency that originates from the decrease in vibrational frequency arising from its larger mass. The change of diffusion coefficient for the precursor should be small because the change in precursor mass is negligible. A lower effusion rate constant allows us to use higher temperatures at the same precursor flux and consequently [Eq. (15)] obtain a lower DB density as shown in Fig. 5. The simulated lines in Fig. 5 could be obtained by simply reducing the hydrogen desorption rates by a factor of 2 corresponding to the

decreased vibration frequencies of a pair of deuterium atoms compared to hydrogen. The high deposition rate saturation defect densities are lowered because the experimentally observed defect densities is a factor of 2 lower in *a*-Si:D compared to *a*-Si:H deposited at 250 °C. From Eq. (12), this implies a lower abstraction rate constant for reaction 6, for deuterated compared to hydrogenated reactants. Given the approximate nature of the simulation, the agreement with the data for the two isotopes at two different temperatures is remarkable. The combination of Figs. 1 and 5 thus constitutes very strong evidence for the growth mechanism illustrated in Fig. 6, and the approximations that we have incorporated in the above discussion.

The other possible surface reactions that affect the DB density on the growth surface are those of hydrogen-atom-assisted abstraction of H from Si-H sites or hydrogen-assisted saturation of DB's, impurity saturation of DB's and recombination of DB's. In order to test the effect of hydrogen atoms on the defect formation process, we diluted silane with hydrogen in different proportions to significantly lower the silane partial pressure that would allow increasing numbers of hydrogen atoms to reach the growing surface without reaction with silane molecules. These results are shown with those for pure silane deposited films prepared at 400 °C in Fig. 1. From the overlap of the data, it seems that at this temperature and range of deposition rates, the net effect of hydrogen atoms on the defect formation process is negligible. This could be due to the reactions



and



reactions having equal rates, which is unlikely because while the rate of reaction (16a) depends on the hydrogenated site density (N_H), that of reaction (16b) depends on the surface DB density (N_s). Unlike N_H , which is relatively unaffected, N_s varies greatly at different deposition rates at 400 °C. The other possibility is that at 400 °C the few physisorbed H atoms react quickly with the physisorbed SiH₃ and desorb as silane. This suppresses the effect of Eqs. (16). Under low SiH₃ flux conditions, for example, those used for microcrystalline material, the physisorbed SiH₃ concentration is low and the effects of Eqs. (16) must be taken into account for obtaining the defect density.

The DB recombination process on the surface can be represented as

$$dN_s/dt = C_{abr}(T)N_s^2 \quad (17)$$

where C_{abr} is the temperature-dependent reaction-rate constant. This process is weak at low N_s and depends on the activated hydrogen hopping process to obtain a pair of DB's on neighboring sites which can recombine as they sink from surface to subsurface. We expect that this process would be a limiting factor at low deposition rates (< 0.2 Å/s) and high surface DB densities, a region that would be interesting to study for confirmation. The im-

purity (oxygen) saturation of DB's on the surface would also be important at low deposition rates when their flux (and hence reaction rates with DB's) would become significant in comparison to the SiH_3 flux (reaction rate with DB's).

Let us now attempt to describe the implications of Figs. 1 and 5 for the thermal equilibrium model of defect formation in *a*-Si:H. It is evident from Eq. (3) that an increase of the growth rate tends to reduce the number of hydrogen, N_H , that are able to participate in the equilibration process by raising E_R [Eq. (3b)]. If we assume that the hydrogen concentration in the plasma increases with power density, the position of μ_H in the film should be raised. This implies a larger number density of mobile hydrogen atoms [from Eq. (2)] as well as an increase in occupancy of the Si—H bonding states. Since the total number of hydrogen atoms which move during the growth of a few monolayers limits equilibration at 250 °C,²³ the combined effects of raising μ_H and E_R with increasing growth rate might annul to keep the number of hydrogen participating in equilibration constant while changing the proportion of Si—H—Si to Si—H bonds. Thus, the defect density could be independent of deposition rate as observed for 250 °C deposited material in Fig. 1. The usual explanation for the observed increase of defect density with applied power under higher pressure deposition conditions⁴⁹ ignores the effect of Eq. (2), considering only Eq. (3).¹² The constancy of E_u in addition to the defect density would suggest that the structure attains equilibrium. The difficulty lies in the growth rate independent hydrogen content¹⁷ which would suggest the μ_H does not change with increasing growth rate and should therefore lead to an increase of the defect density, contrary to observations (Fig. 1).

Increasing the temperature has the effect of speeding up the diffusion of mobile hydrogen for completion of reaction 1, of increasing the number of mobile hydrogen via Eq. (2), and of lowering E_R at the same growth rate [Eq. (3)]. The increase in equilibration rate at 400 °C compared to 250 °C changes the constraints on the defect density. A lowering of μ_H due to faster effusion of hydrogen serves to enhance the number of DB's by depopulation of the Si—H bonds. Further, at the higher temperature, disorder and hence the strained bond density is also expected to increase⁵² and should result in a higher density of DB's at the same deposition rates. The decrease of the defect density on increasing the growth rate that is observed at 400 °C is inconsistent with expectations of the concept of thermal equilibration. Further, substituting D for H should slow down the equilibration process (reaction 1) due to slower diffusion and result in a higher defect density, contrary to observations (Fig. 5).

One expects that if there is indeed any equilibration between strained and weak bonds, this should be attained during the cooling process. The defect densities have been plotted as a function of E_u in Fig. 4 along with the lines showing the calculated defect densities for two different equilibrium temperatures from Fig. 12 in Ref. 21. We find that the data lie between the curves for equilibration temperatures of 200 and 400 K which is much too low compared to temperatures quoted for un-

doped material (~ 500 K).²² We may conjecture that the structure of the material is modified when deposited at 400–450 °C compared to 250 °C such that defect formation energies are larger and therefore a smaller density of defects are formed from similar densities of strained bonds (E_u) for similar cooling rates and freeze-in temperatures.²² However, a decrease in the hydrogen content in higher-temperature-deposited material would be expected to raise the equilibration temperature. The observed decrease in the value of E_u with increasing growth rate¹⁷ is fundamentally contradictory to the concept of TE. The confusion is confounded by the fact that the Raman linewidth that is usually associated with the bond angle disorder⁵³ does not change when the deposition rate changes or the temperature increases, consistent with a previous report.⁵⁴ Moreover, the minimum value of E_u is clearly not determined by the temperature²⁵ since at the highest deposition rates, E_u decreases below kT at 400 °C. The hydrogen diffusion-limited equilibration in the growth zone should lead to a growth-rate-dependent hydrogen concentration but this is not observed.¹⁷ In fact, the existence of the growth zone is unlikely in view of the fact that the hydrogen-rich surface is only a monolayer thick.^{4,26} Therefore we are drawn to the conclusion that the thermal equilibration mechanism does not apply to the defects formed during growth.

VI. CONCLUSIONS

The defect density in *a*-Si:H has been shown to remain unchanged on increasing the deposition rate by almost two orders of magnitude at 250 °C. At higher temperatures, the defect density has been shown to decrease systematically with increasing deposition rate. These results have been shown to evolve naturally from the surface diffusion process of growth precursors having low reactivity on a hydrogen terminated surface. Thus, the concept of bulk defects being formed on the growth surface and becoming statistically incorporated in the film has been established. Isotopic substitution has been shown to modify the defect formation rates, as expected from the surface-controlled defect formation process. It has been shown that the results contradict expectations from the thermal equilibration mechanism that has been proposed to determine the bulk defect density in *a*-Si:H. It is expected that the defect density in *a*-Si:H can be reduced by finding ways to enhance the precursor diffusion length on the growth surface.

ACKNOWLEDGMENTS

We would like to thank Dr. J. Isoya of the University of Library and Information Sciences for the ESR measurements, Dr. K. Murayama of Nihon University for the TOF measurements, and Dr. S. Hayashi of the National Chemical Laboratory for Industry for the NMR measurements. We thank Dr. I. Sakata for the use of CPM and ESR spectrometers. It is a pleasure to thank Dr. N. Hata for critical reading of the manuscript and useful discussions. We are grateful to Dr. K. Tanaka for his continued interest and perceptive comments regarding this work.

- ¹See, for example, M. Hirose, in *Semiconductors and Semimetals*, edited by J. I. Pankove (Academic, Orlando, 1984), Vol. 21, Pt. A, p. 9.
- ²See, for example, K. Tanaka and A. Matsuda, *Mater. Sci. Rep.* **2**, 139 (1987); *Semiconductors and Semimetals* (Ref. 1), Vol. 21, Pt. A, pp. 153–222.
- ³A. Matsuda, in *Proceedings of the International Seminar on Reactive Plasmas*, edited by T. Goto (Nagoya University, Japan, 1991), p. 405.
- ⁴Y. Toyoshima, K. Arai, A. Matsuda, and K. Tanaka, *J. Non-Cryst. Solids* **137/138**, 765 (1991).
- ⁵T. Shirafuji, M. Yoshimoto, T. Ffuyuki, and H. Matsunami, *Jpn. J. Appl. Phys.* **30**, L538 (1991).
- ⁶T. D. Moustakas, in *Semiconductors and Semimetals* (Ref. 1), Vol. 21, Pt. A, p. 55; M. Pinarbasi, N. Maley, A. Myers, and J. R. Abelson, *Thin Solid Films* **171**, 217 (1989).
- ⁷H. Curtins, N. Wyrsh, M. Favre, K. Prasad, M. Brechet, and A. V. Shah, *Proc. Mater. Res. Soc. Symp.* **95**, 249 (1987).
- ⁸N. M. Johnson, J. Walker, and K. S. Stevens, *J. Appl. Phys.* **69**, 2631 (1991).
- ⁹A. H. Mahan, J. Carapella, B. P. Nelson, R. S. Crandall, and, I. Balberg, *J. Appl. Phys.* **69**, 6728 (1991).
- ¹⁰Z. E. Smith and S. Wagner, *Phys. Rev. B* **32**, 5510 (1985).
- ¹¹K. Winer, *Phys. Rev. B* **41**, 7952 (1990).
- ¹²Z. E. Smith and S. Wagner, *Phys. Rev. Lett.* **59**, 688 (1987).
- ¹³A. Matsuda, *J. Non-Cryst. Solids* **59/60**, 767 (1983).
- ¹⁴A. Matsuda and K. Tanaka, *J. Non-Cryst. Solids* **97/98**, 1367 (1987).
- ¹⁵Hong Yan, *Phys. Rev. Lett.* **68**, 3048 (1992).
- ¹⁶Y. M. Li, I. An, H. V. Nguy, C. R. Wronski, and R. W. Collins, *Phys. Rev. Lett.* **68**, 2814 (1992).
- ¹⁷G. Ganguly and A. Matsuda, *Mater. Res. Soc. Symp. Proc.* **258**, 39 (1992); *Jpn. J. Appl. Phys.* **31**, L1269 (1992).
- ¹⁸R. A. Street, *Phys. Rev. Lett.* **49**, 1187 (1982).
- ¹⁹K. Pierz, W. Fuhs, and H. Mell, *J. Non-Cryst. Solids* **114**, 651 (1989).
- ²⁰R. A. Street, J. Kakalios, and T. M. Hayes, *Phys. Rev. B* **34**, 3030 (1986).
- ²¹R. A. Street and K. Winer, *Phys. Rev. B* **40**, 6236 (1989).
- ²²T. J. McMahon, *Solar Cells* **30**, 235 (1991).
- ²³R. A. Street, *Phys. Rev. B* **43**, 2454 (1991); **44**, 10 610 (1991).
- ²⁴A. Matsuda, S. Yokoyama, and K. Tanaka, *Appl. Phys. Lett.* **53**, 1489 (1988).
- ²⁵M. Stutmann, *Philos. Mag. B* **60**, 531 (1989).
- ²⁶R. Robertson, D. Hils, H. Chatham, and A. Gallagher, *Appl. Phys. Lett.* **43**, 544 (1983).
- ²⁷R. Robertson and A. Gallagher, *J. Appl. Phys.* **59**, 3402 (1986).
- ²⁸P. A. Longeway, H. A. Weakleim, and R. D. Estes, *J. Phys. Chem.* **88**, 3282 (1984).
- ²⁹N. Itabashi, K. Kata, N. Nishikawa, T. Goto, C. Y. Yamada, and E. Hirota, *Jpn. J. Appl. Phys.* **27**, L1567 (1988).
- ³⁰A. Matsuda and K. Tanaka, *Thin Solid Films* **92**, 171 (1982).
- ³¹K. Tachibana, *Proceedings of the International Seminar on Reactive Plasmas* (Ref. 3), p. 399.
- ³²N. Itabashi, N. Nishiwaki, M. Magane, S. Naito, T. Goto, A. Matsuda, C. Yamada, and E. Hirota, *Jpn. J. Appl. Phys.* **29**, L505 (1990).
- ³³The “physisorption” state of the radicals is a loosely bound condition that allows them to move more freely (small activation energy of ~ 0.3 eV) than if they were chemisorbed as with silicon self-diffusion activation energies of ~ 0.7 eV cf. Y. Mo, J. Kellner, M. B. Webb, and M. Lagally, *Phys. Rev. Lett.* **66**, 1998 (1991).
- ³⁴A. Matsuda, K. Nomoto, Y. Takeuchi, A. Suzuki, A. Yuuki, and J. Perrin, *Surf. Sci.* **227**, 50 (1990).
- ³⁵Y. Toyoshima, K. Arai, A. Matsuda, and K. Tanaka, *Appl. Phys. Lett.* **56**, 1540 (1990); **57**, 1028 (1990).
- ³⁶N. Blayo and B. Drevillon, *Appl. Phys. Lett.* **57**, 786 (1990).
- ³⁷J.-L. Guizot, K. Nomoto, and A. Matsuda, *Surf. Sci.* **244**, 22 (1991).
- ³⁸A. Matsuda and K. Tanaka, *J. Appl. Phys.* **60**, 2351 (1986).
- ³⁹A. Nuruddin, J. R. Doyle and J. R. Abelson, *Mater. Res. Soc. Symp. Proc.* **258**, 33 (1992).
- ⁴⁰J. P. Conde, K. K. Chan, J. M. Blum, M. Arienzo, and J. J. Cuomo, *J. Appl. Phys.* **71**, 3981 (1992).
- ⁴¹M. Hoheisel, O. Stika, and J. Kocka, *J. Non-Cryst. Solids* **137/138**, (1991).
- ⁴²C. R. Wronski, Z. E. Smith, S. Aljishi, V. Chu, K. Shepard, D. S. Shen, R. Schwarz, D. Slobodin, and S. Wagner, in *Stability of Amorphous Silicon Alloy Materials and Devices*, edited by B. L. Stafford and E. Sabisky, AIP Conf. Proc. No. 157 (AIP, New York, 1987), p. 70; Z. E. Smith, V. Chu, K. Shepard, S. Aljishi, D. Slobodin, J. Kolodzey, S. Wagner, and T. L. Chu, *Appl. Phys. Lett.* **50**, 1521 (1991).
- ⁴³N. Wyrsh, F. Finger, T. J. McMahon, and M. Vanecek, *J. Non-Cryst. Solids* **137/138**, 347 (1991).
- ⁴⁴M. Vanecek, J. Kocka, J. Stuchlik, Z. Kozisek, O. Stika, A. Triska, *Solar Energy Mater* **8**, 411 (1983).
- ⁴⁵T. Shimizu, H. Kidoh, A. Morimoto, and M. Kumeda, *Jpn. J. Appl. Phys.* **28**, 586 (1989).
- ⁴⁶F. Siebke, W. Beyer, J. Herion, and H. Wagner, *J. Non-Cryst. Solids* **137/138**, 339 (1991); A. Asano and M. Stutzmann, *ibid.* **137/138**, 623 (1991).
- ⁴⁷M. Favre, A. Shah, J. Hubin, E. Bustarret, M. A. Hachicha, and S. Basrour, *J. Non-Cryst. Solids* **137/138**, 335 (1991).
- ⁴⁸Y.-Jia, A. Yamada, M. Konagai, and K. Takahashi, *Jpn. J. Appl. Phys.* **30**, 893 (1991).
- ⁴⁹W. B. Jackson and N. Amer, *Phys. Rev. B* **25**, 5559 (1982).
- ⁵⁰D. S. Shen, H. Chatham, and P. K. Bhat, *Solar Cells* **30**, 271 (1991).
- ⁵¹The reason why higher power densities could not be used is due to fluctuation of the plasma. At high generation rates within the interelectrode space, there is an outward flux of dissociated species which is countered by an inward flux of silane molecules necessary to maintain the same level of dissociation. At higher power levels this leads to severe fluctuations of the plasma near the edge which can be seen even by the naked eye.
- ⁵²Y. Bar-Yam, D. Adler, and J. D. Joannopoulos, *Phys. Rev. Lett.* **57**, 467 (1986).
- ⁵³J. S. Lanin, in *Semiconductors and Semimetals* (Ref. 1), Vol. 21, Pt. B, p. 159.
- ⁵⁴K. Watanabe, S. Tsuda, M. Ohnishi, and Y. Kuwano, *Jpn. J. Appl. Phys.* **24**, 385 (1985).